PcxL and HpxL are flavin-dependent, oxime-forming *N*-oxidases in phosphonocystoximic acid biosynthesis in *Streptomyces*

Received for publication, January 2, 2018, and in revised form, March 12, 2018 Published, Papers in Press, March 14, 2018, DOI 10.1074/jbc.RA118.001721

Michelle N. Goettge[‡], Joel P. Cioni[‡], Kou-San Ju[‡1], Katharina Pallitsch[§], and William W. Metcalf[‡2]

From the [‡]Department of Microbiology and the Carl R. Woese Institute for Genomic Biology, University of Illinois Urbana-Champaign, Urbana, Illinois 61801 and the [§]Institute of Organic Chemistry, University of Vienna, 1090 Vienna, Austria

Edited by Ruma Banerjee

Several oxime-containing small molecules have useful properties, including antimicrobial, insecticidal, anticancer, and immunosuppressive activities. Phosphonocystoximate and its hydroxylated congener, hydroxyphosphonocystoximate, are recently discovered oxime-containing natural products produced by *Streptomyces* sp. NRRL S-481 and *Streptomyces regensis* NRRL WC-3744, respectively. The biosynthetic pathways for these two compounds are proposed to diverge at an early step in which 2-aminoethylphosphonate (2AEPn) is converted to (*S*)-1-hydroxy-2-aminoethylphosphonate ((*S*)-1H2AEPn) in *S. regensis* but not in *Streptomyces* sp. NRRL S-481). Subsequent installation of the oxime moiety into either 2AEPn or (*S*)-1H2AEPn is predicted to be catalyzed by PcxL or HpxL from *Streptomyces* sp. NRRL S-481 and *S. regensis* NRRL WC-3744, respectively, whose sequence and predicted structural characteristics suggest they are unusual *N*-oxidases. Here, we show that recombinant PcxL and HpxL catalyze the FAD- and NADPH-dependent oxidation of 2AEPn and 1H2AEPn, producing a mixture of the respective aldoximes and nitrosylated phosphonic acid products. Measurements of catalytic efficiency indicated that PcxL has almost an equal preference for 2AEPn and (*R*)-1H2AEPn. 2AEPn was turned over at a 10-fold higher rate than (*R*)-1H2AEPn under saturating conditions, resulting in a similar but slightly lower k_{cat}/K_m. We observed that (*S*)-1H2AEPn is a relatively poor substrate for PcxL but is clearly the preferred substrate for HpxL, consistent with the proposed biosynthetic pathway in *S. regensis*. HpxL also used both 2AEPn and (*R*)-1H2AEPn, with the latter inhibiting HpxL at high concentrations. Bioinformatic analysis indicated that PcxL and HpxL are members of a new class of oxime-forming *N*-oxidases that are broadly dispersed among bacteria.

This work was supported by National Institutes of Health Grant P01 GM077596 B from NIGMS and Grant P27987-N28 from the Austrian Science Fund (FWF). The authors declare that they have no conflicts of interest with the contents of this article. The content is solely the responsibility of the authors and does not necessarily represent the official views of the National Institutes of Health.

This article contains Figs. S1–S6 and Table S1.

[1] Present address: Dept. of Microbiology and Div. of Medicinal Chemistry and Pharmacognosy, Ohio State University, Columbus, OH 43210.

[2] To whom correspondence should be addressed. Tel.: 217-244-1943; Fax. 217-244-6697; E-mail: metcalf@illinois.edu.

Oxime-containing small molecules often possess useful biological properties, including antibacterial (1), antifungal (2), insecticidal (3, 4), antitumor (5), immunosuppressive (6), and acetylcholinesterase reactivation activities (7, 8). Some of these bioactive oximes are natural products, with the most commonly identified being the glucosinolates (Fig. 1). These amino acid–derived natural products, produced by plants of the order Capparales, contain a sulfonated oxime responsible for the distinctive flavor and odor of many cruciferous vegetables (9). Other natural product oximes include the vibralactoximes, which are biosynthetic derivatives of the lipase inhibitor vibralactone, produced by the fungus *Boreostereum vibrans* (10); the DNA methyltransferase inhibitor psammaplin A, produced by the sea sponge *Psammaplinaplysilla* (11); and the β-lactam antibiotic nocardicin A, produced by the actinobacterium *Nocardia uniformis* subsp. *tsuyamanesis* (1) (Fig. 1).

Three different enzyme families are known to produce oxime moieties: (1) cytochrome P450–dependent monooxygenases, (2) ferritin-like enzymes, and (3) flavin-dependent *N*-monooxygenases. Glucosinolates are usually made via a pathway involving a cytochrome P450–dependent monooxygenase that catalyzes successive *N*-oxidations to yield an oxime derivative of an amino acid (9, 12); however, these molecules are probably made via an unknown FAD-NAD(P)H-dependent oxygenase in *Brassica napus* and *Brassica camestris* (13, 14). In bacteria, the oxime in nocardicin A is installed by a cytochrome P450–dependent monooxygenase known as NocL (1, 15), whereas a metal-dependent *N*-oxygenase, AlmD, is responsible for oxime formation in althiomycin (16). Finally, the oxime in the ribosomally synthesized peptide azolemycin is post-translationally installed by the flavin-dependent monooxygenase AzmF (17), whereas the oxime in caerulomycin A is introduced using a two-component flavin-dependent monooxygenase, CrmH (18).

Our laboratory recently identified two new phosphonate natural products with an unusual thiohydroximate moiety (19). These include phosphonocystoximic acid, produced by *Streptomyces* sp. NRRL S-481, and its hydroxylated congener, hydroxyphosphonocystoximic acid, made by a number of *Streptomyces* species, including *Streptomyces regensis* NRRL WC-3744, which also makes hydroxynitrilaphos (20). Significantly, many hydroxyphosphonocystoximate producers make small amounts of phosphonocystoximic acid, as well as a suite of biosynthetic intermediates that differ solely by hydroxylation

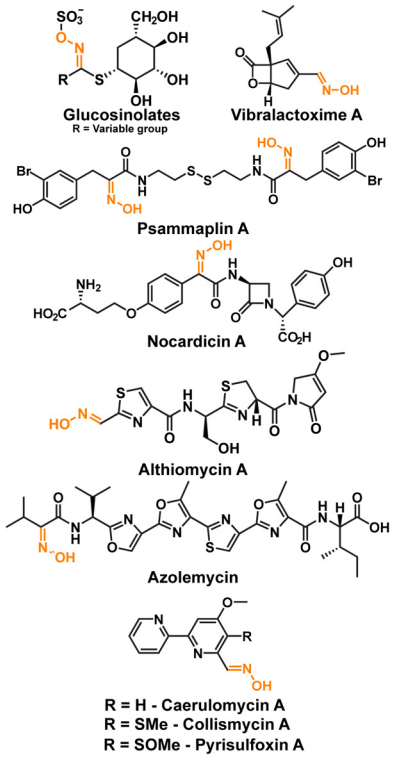

Figure 1. Oxime-containing natural products.

at the carbon α to the phosphorus atom, suggesting that similar molecular machinery is used to produce both natural products (19). This idea is strongly supported by analysis of the biosynthetic genes clusters associated with production of these oxime-containing natural products.

Eighteen genes are shared between the clusters responsible for the synthesis of phosphonocystoximate (the *pcx* gene cluster) and hydroxyphosphonocystoximate (the *hpx* gene cluster) based on significant amino acid identity between the encoded proteins (Fig. S1 and Table S1). The first nine genes (*hpxA–I* and *pcxA–I*) in both clusters are highly homologous and found in the same order. Nine additional genes are also shared between the two clusters, with their organization conserved for the most part (*pcxK–pcxU* and *hpxK–hpxU*). Thus, it seems likely that most of the biosynthetic steps required for synthesis of the two congeners are similar. However, the gene clusters also show significant differences. Key among these differences is a gene encoding a putative 2-oxoglutarate– dependent dioxygenase designated HpxV, found solely in *S. regensis*. Based on the presence of this gene and the observed metabolic intermediates produced by the two strains, a scheme for biosynthesis of phosphonocystoximate and hydroxyphosphonocystoximate biosynthesis was proposed (Fig. 2 and Ref. 19). The proposed pathways diverge at an early step, with hydroxylation of 2AEPn[3] by HpxV yielding 1H2AEPn solely in *S. regensis*. Consistent with this model, we recently found that purified HpxV catalyzes this reaction, generating the *S*-enantiomer of

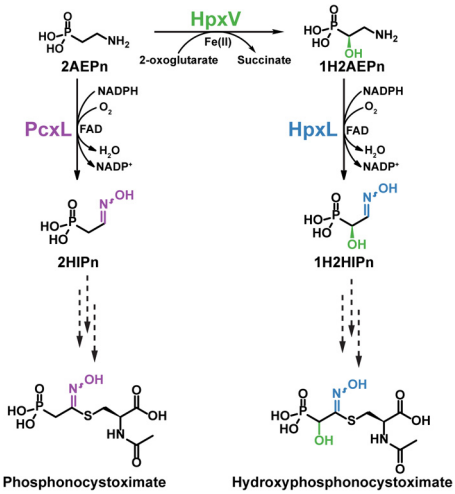

Figure 2. The proposed biosynthetic route of oxime formation in phosphonocystoximates. HpxV is a 2-oxoglutarate- and ferrous iron-dependent 2AEPn dioxygenase that converts 2AEPn to (*S*)-1H2AEPn. PcxL and HpxL are FAD- and NADPH-dependent amine oxidases that catalyze 2AEPn or 1H2AEPn oxidation to yield 2-hydroxyiminoethylphosphonic acid (**1**) and 1-hydroxy-2-hydroxyiminoethylphosphonic acid (**3**), respectively. Multiple steps are required to convert these oxime-containing intermediates to the final products (*dashed-line arrows*).

1H2AEPn.[4] The mechanism of oxime formation in the two pathways, however, remains a mystery, because homologs of known oxime-forming enzymes are not found in either biosynthetic gene cluster. Nevertheless, putative NAD(P)H-dependent and flavin-dependent oxygenases produced by the *pcxL* and *hpxL* genes in *Streptomyces* sp. NRRL S-481 and *S. regensis*, respectively, have been suggested as possible candidates for this enzymatic activity (19).

Here we present *in vitro* biochemical evidence that supports this proposal. The data reveal PcxL and HpxL as the founding members of a novel family of oxime-forming enzymes required for the production of the hydroxylated and nonhydroxylated forms of thiohydroximate phosphonic acid natural products.

Results

Bioinformatic analysis suggests that HpxL and PcxL are novel oxime-forming amine oxygenases

Several lines of bioinformatics evidence suggest that the PcxL and HpxL proteins are responsible for the installation of the oxime moiety in the phosphonocystoximic acids produced by *Streptomyces* sp. S-481 and *S. regensis*. First, conserved FAD- and NAD(P)-binding domains are observed in both proteins, consistent with a role in redox chemistry. Second, both have a structural similarity to the N-terminal domain of L-ornithine *N*-hydroxylase from *Pseudomonas* (Protein Data Bank entry 3S5W) and *Kutzneria* (Protein Data Bank entry 4TLX) based on the protein-fold recognition algorithm, Phyre2 (21). Taken together, these data suggest that PcxL and HpxL may catalyze FAD- and NAD(P)-dependent amine oxidation. Additional support for the proposed amine oxidase function is provided by their weak similarity (~35% identity) to the FAD-NAD(P)H-dependent enzymes involved in the biosynthetic pathways of

[3] The abbreviations used are: 2AEPn, 2-aminoethylphosphonate; 1HAEPn, 1-hydroxy-2-aminoethylphosphonate; PepM, phosphoenolpyruvate mutase; TEV, tobacco etch virus.

[4] M. N. Goettge and W.W. Metcalf, unpublished data.

Table 1

Known characterized *N*-oxidases and their homology to HpxL, which is encoded by the hydroxyphosphonocystoximic gene cluster

PcxL is found in the homologous phosphonocystoximic biosynthetic gene cluster. FzmM and CreE catalyze the *N*-oxidation of aspartic acid to nitrosuccinic acid during fosfazinomycin and cremeomycin biosynthesis, respectively (22, 23). AzmF and CrmH are characterized as flavin-dependent *N*-oxidases that catalyze oxime formation in azolemycin and caerulomycin biosynthesis (17, 18). ClmM is the predicted FAD- and NAD(P)H-dependent *N*-oxidase of collismycin biosynthesis (40), and AlmD is the metal-dependent *N*-oxidase involved in oxime formation of alithomycin biosynthesis (16). Note that only FzmM and CreE can be considered *bona fide* homologs of PcxL and HpxL.

Enzyme	NCBI accession no.	Organism	Natural product	% Identity to HpxL	*E*-Value	Length[a]
HpxL	WP_030990682.1	*S. regensis* WC-3744	Hydroxyphosphonocystoximate	100	0	750
PcxL	WP_051704824.1	*Streptomyces* sp. S-481	Phosphonocystoximate	61	0	742
AzmF	AMQ23503.1	*Streptomyces* sp. FXJ1.264	Azolemycin	10	2.9	389
ClmM	CCC55915.1	*Streptomyces* sp. CS40	Collismycin A	9	1.4	402
CrmH	AFD30961.1	*Actinoalloteichus* sp. WH1-2216-6	Caerulomycin A	8	1.1	407
AlmD	CCA29200.1	*Myxococcus xanthus* DK897	Althiomycin	8	3.4	331
FzmM	WP_053787792.1	*Streptomyces* sp. XY332	Fosfazinomycin	30	6*E*-14	644
CreE	ALA99202.1	*Streptomyces cremeus*	Cremeomycin	35	3*E*-29	666

[a] Number of amino acids.

cremeomycin (22) and fosfazinomycin (23) (Table 1). These enzymes oxidize the primary amine of aspartic acid to form nitrosuccinic acid, which is believed to serve as the substrate for downstream *N*–*N* bond formation (22). Finally, the existence of the characterized oxime-forming FAD- and NAD(P)H-dependent amine monooxygenases in the biosynthetic pathways of azolemycin (AzmF) (17) and caerulomycin A (CrmH) (18) is also consistent with the proposed amine oxidase function for PcxL and HpxL. However, it should be stressed that AzmF and CrmH are not related to PcxL and HpxL, based on a comparison of their primary amino acid sequences (Table 1). Moreover, these proteins are significantly smaller than PcxL and HpxL (389 and 407 amino acids *versus* 742 and 750 amino acids). Similarly, the human liver flavin-containing monooxygenases FMO1 (NCBI accession number NP_001269621.1) and FMO3 (NCBI accession number NP_008825.4), which oxidize phenethylamine to the oxime (24), show no similarity to HpxL and PcxL. Thus, if PcxL and HpxL are indeed FAD-NAD(P)H-dependent enzymes that catalyze oxime formation, they belong to a novel protein family.

HpxL and PcxL catalyze NADPH oxidation in the presence of FAD and 2AEPn

To examine the biochemical properties of PcxL and HpxL, His_6 affinity-tagged alleles were overexpressed in *Escherichia coli*. Recombinant proteins were then purified and assayed for their ability to oxidize nicotinamide cofactors in the presence of 2AEPn, FAD, or FMN (Table 2). Both enzymes catalyze the oxidation of NADPH and NADH at a significant rate in the absence of additional substrates. Oxidation of reduced nicotinamides is stimulated by the addition of FAD but not by the addition of FMN, suggesting that the former is the preferred cofactor. It should be noted that the as-purified enzymes contain bound FAD, as indicated by the bright yellow coloration of the preparations (Fig. S2*A*). Additionally, mass spectrometric analysis corroborates the presence of FAD in these protein (Fig. S2, *B–E*), whereas UV-visible spectra clearly show the presence of a flavin that is reduced upon the addition of NADPH (Fig. S2, *F–H*). We believe the presence of FAD bound to the proteins upon purification accounts for the basal activity seen in the absence of added FAD. Significantly, oxidation of NADPH, but not NADH, is substantially increased upon the addition of 2AEPn, with the highest rates observed for the combination

Table 2

Oxidation of nicotinamide cofactors by HpxL and PcxL

The apparent rate in the presence/absence of different flavin cofactors and 2AEPn is shown. **2AEPn*** = rate in the presence of 2AEPn after subtraction of the uncoupled rate (*i.e.* before the addition of 2AEPn). 2AEPn was used at a concentration of 5 mM, whereas FAD and FMN were used at 50 μM and NADPH and NADH at 300 μM. Each experiment was completed in triplicate.

Cofactor(s)	Substrate	k_{obs} HpxL	k_{obs} PcxL
		$s^{-1} \times 10^{-3}$	
NADPH	None	2.7 ± 0.4	14.4 ± 0.7
	2AEPn	7.2 ± 0.6	232 ± 8
NADPH/FAD	None	12.5 ± 0.1	21 ± 1
	2AEPn	23.2 ± 0.7	310 ± 20
	2AEPn*	**10.7 ± 0.6**	**290 ± 20**
NADPH/FMN	None	5.2 ± 0.5	14.3 ± 0.7
	2AEPn	10.0 ± 0.2	210 ± 20
	2AEPn*	**4.8 ± 0.7**	**200 ± 20**
NADH	None	5.5 ± 0.1	24 ± 1
	2AEPn	1.7 ± 0.2	29 ± 2
NADH/FAD	None	14 ± 2	85 ± 5
	2AEPn	15.0 ± 0.7	83 ± 5
	2AEPn*	**0.1 ± 0.1**	**0 ± 3**
NADH/FMN	None	5.9 ± 0.3	26.6 ± 0.2
	2AEPn	7.0 ± 0.4	27 ± 4
	2AEPn*	**1.0 ± 0.2**	**1 ± 4**

of NADPH, FAD, and 2AEPn. Thus, activity in the absence of 2AEPn is likely due to an uncoupled, oxygen-dependent reaction, which is common for flavin-dependent enzymes (25). Additionally, when this reaction is run in the absence of oxygen, there is no oxidation of NADPH by PcxL in either the presence or absence of 2AEPn (data not shown).

HpxL and PcxL oxidize 2AEPn to 2-hydroxyiminoethylphosphonic acid and 2-nitroethylphosphonic acid

A series of NMR experiments were conducted to establish the products of PcxL- and HpxL-catalyzed 2AEPn oxidation. Based on ^{31}P NMR spectroscopy, both enzymes form three phosphorus-containing products after prolonged incubation with NADPH, FAD, and 2AEPn (Fig. 3, *A* and *B*). Analysis of these molecules using proton-phosphorus–coupled HMBC NMR spectroscopy allowed assignment of the major peak as a mixture of the (*E*)- and (*Z*)-isomers of 2-hydroxyiminoethylphosphonic acid (**1**), with smaller amounts of 2-nitroethylphosphonic acid (**2**) (Figs. S3 and S4). Accordingly, aldoxime protons display a characteristic proton NMR spectroscopy chemical shift that will be between 6.5 and 8.0 ppm (26). A

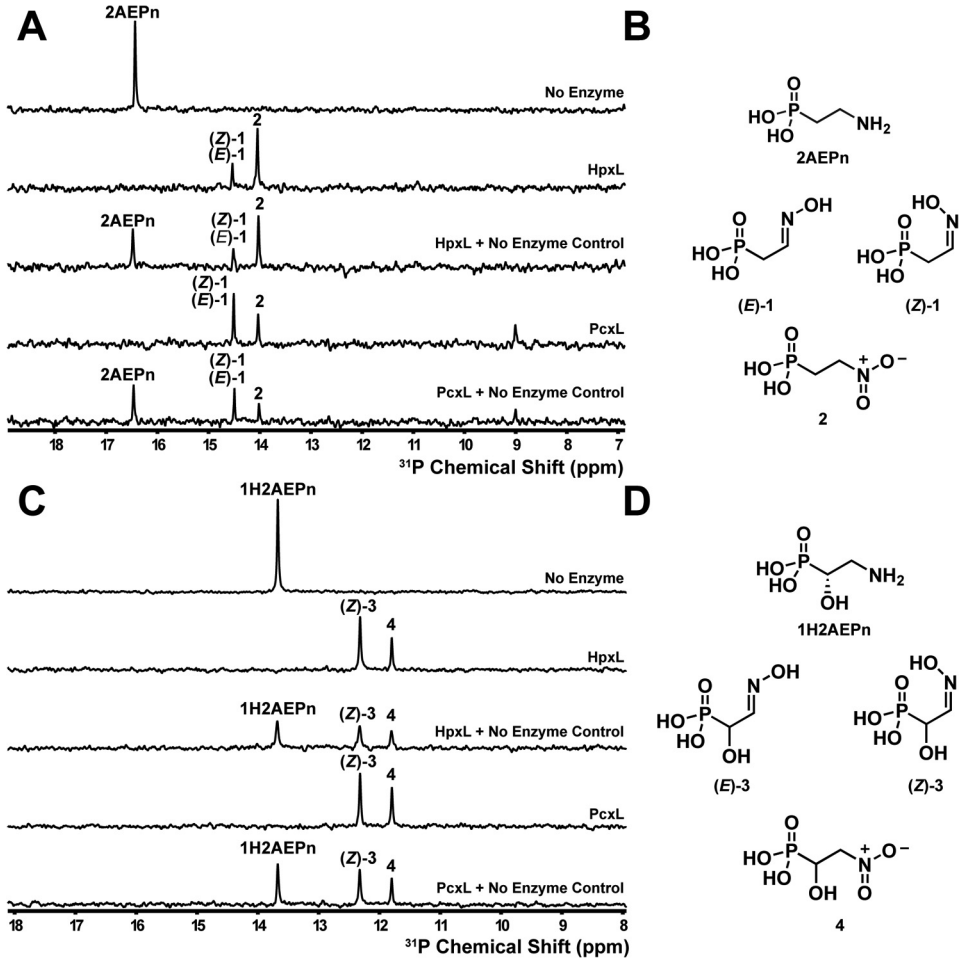

Figure 3. Phosphorus NMR spectroscopy analysis of *N*-oxidase activity in the presence of 2AEPn or (*S*)-1H2AEPn. *A*, HpxL and PcxL form three major products *in vitro* when incubated for 16 h with NADPH, FAD, and 2AEPn as the substrate, whereas no product formation is observed in the absence of enzyme. *B*, these products have been assigned as the (*E*)- and (*Z*)-isomers of 2-iminoethylphosphonic acid (**1**) and 2-nitroethylphosphonic acid (**2**) based on the ^{1}H-^{31}P HMBC analysis (Figs. S2 and S3). Note that the (*E*)- and (*Z*)-isomers of **1** have identical ^{31}P chemical shifts and thus display only a single peak in the one-dimensional ^{31}P spectrum shown in *A*. *C*, HpxL and PcxL both generate two products *in vitro* using (*S*)-1H2AEPn as the substrate. *D*, these products were assigned as (*Z*)-1-hydroxy-2-hydroxyiminoethylphosphonic acid (**3**) and 1-hydroxy-2-nitroethylphosphonic acid (**4**) based on the ^{1}H-^{31}P HMBC analysis (Fig. S4 and S5). Chemical-mixing experiments with the control reaction were performed to confirm that substrate had been completely consumed. Substrates and cofactors were added at the following concentrations: 100 μM FAD, 500 μM NADPH, 3 mM 2AEPn or HpxV-generated (*S*)-1H2AEPn, 25 μM PcxL or HpxL, 25 mM phosphite, and 10 μM PTDH17x.

single proton associated with each of the products, which we assigned as (*E*)-**1** and (*Z*)-**1** at 6.82 and 7.37 ppm, respectively. This assignment is supported by a recent report of the total synthesis of the phosphonocystoximic acids, which involves the synthesis of ethyl-protected aldoximes as intermediates (27). The aldoxime protons for the protected (*E*)-isomer have a chemical shift of 6.82 ppm, whereas the aldoxime proton associated with the protected (*Z*)-isomer has a chemical shift of 7.41 ppm (27). Our assignment of the third product as 2-nitroethylphosphonic acid (**2**) is based on the observation of phosphorus-correlated protons at 2.03 and 4.48 ppm, which is consistent with literature values of synthetically produced 2-nitroethylphosphonic acid (28). Although both enzymes form a mixture of (*E*)- and (*Z*)-isomers when using 2AEPn as substrate, HpxL preferentially forms (*E*)-**1** (Fig. S3), whereas PcxL preferentially forms (*Z*)-**1** (Fig. S4).

We performed an identical experiment using 1H2AEPn as substrate to determine the products that would be formed by the enzymes. PcxL and HpxL catalyze oxidation of the amine moiety in (*S*)-1H2AEPn as a substrate (Fig. 3, *C* and *D*). In contrast to the products obtained with 2AEPn, the enzymes form only the (*Z*)-isomer of 1-hydroxy-2-hydroxyiminoethylphosphonic acid (**3**) when using (*S*)-1H2AEPn as the substrate. This is evident by the presence of only one set of protons correlating with the phosphorus atom with chemical shifts of 4.15 and 7.44 ppm (Figs. S5 and S6). The enzymes also form smaller amounts of 1-hydroxy-2-nitroethylphosphonic acid (**4**) (Figs. S5 and S6).

To determine the molar ratio of substrates consumed to cofactor used, we determined the stoichiometry of the reaction by monitoring substrate (2AEPn and oxygen) and cofactor (NADPH) consumption during short incubations. We observed that the molar ratio of oxygen to NADPH was ~1:1 for both enzymes; however, the molar ratio of NADPH to 2AEPn consumption was much higher: 2.5:1 (NADPH/2AEPn) for PcxL and 4.0:1 for HpxL (Table 3). This yields an overall reaction stoichiometry of 2AEPn to NADPH to oxygen consumption of 1/2.5/2.7 for PcxL and 1/4.0/3.8 for HpxL. Signifi-

Table 3
Stoichiometry of PcxL- and HpxL-catalyzed reactions
Oxygen and NADPH consumption was measured in 5-min reactions using a Clark-type electrode and UV/visible spectrophotometry, respectively, to determine the O_2/NADPH ratio. A separate 3-h reaction was used to obtain the NADPH/2AEPn ratio with ^{31}P NMR used to monitor both substrates. Each experiment was performed in triplicate.

		O_2/NADPH			NADPH/2AEPn			Combined ratio
Substrate	Enzyme	nmol NADPH	nmol O_2	Ratio	nmol NADPH	nmol 2AEPn	Ratio	2AEPn/ O_2/NADPH
2AEPn	PcxL	966 ± 0.4	1040 ± 2	1:1.1	1970 ± 3	810 ± 30	2.5:1	1:2.5:2.7
	HpxL	163 ± 1	156 ± 2	1.1:1	1420 ± 30	350 ± 50	4.0:1	1:4.0:3.8

cantly, **2** was not observed during the short incubations used in these experiments (data not shown). Thus, the presence of this product in longer incubations is probably due to overoxidation of the substrate.

HpxL and PcxL both preferentially oxidize 1H2AEPn over 2AEPn but with different stereochemical preferences

To determine the substrate preference of the *N*-oxidases *in vitro*, we performed initial rate kinetics on PcxL and HpxL using 2AEPn and the (*R*)- and (*S*)-enantiomers of 1H2AEPn as substrates (Table 4 and Fig. 4). Although both enzymes are capable of using all of these substrates, they manifest significantly different substrate preferences. PcxL shows the highest rate with 2AEPn as substrate, but it shows a greater affinity for (*R*)-1H2AEPn. Thus, the catalytic efficiency of PcxL is similar for these two substrates. In contrast, (*S*)-1H2AEPn is a relatively poor substrate for PcxL, whereas HpxL turns over (*S*)-1H2AEPn and 2AEPn at similar rates but has a 10-fold higher affinity for the former. Thus, (*S*)-1H2AEPn, which is predicted to be the *in vivo* substrate, is the preferred substrate for this enzyme. (*R*)-1H2AEPn is a relatively poor HpxL substrate and actually inhibits the enzyme at higher concentrations (Fig. 4*F*).

HpxL and PcxL are members of a large family of putative N-oxidases that is common in phosphonate biosynthetic pathways

The low similarity of HpxL and PcxL to other known *N*-oxidases suggests that they are members of larger protein family (Table 1). Indeed, BLAST searches of GenBank™ retrieved thousands of hits using HpxL and PcxL as query sequences (data not shown). Phylogenetic analysis of the top 500 HpxL homologs reveals numerous discrete clades within the family. To provide clues as to the function of the proteins within this family, we examined the genomic context surrounding these homologs using the bioinformatics tool RODEO, which retrieves adjacent genes and assigns putative functions based on PFAM membership (29). Significantly, almost all genes encoding proteins within the HpxL and PcxL clade fall within gene clusters devoted to the synthesis of phosphonic acids based on co-localization with genes encoding phosphoenolpyruvate mutase (PepM), which encodes the first step in most phosphonate biosynthetic pathways (Fig. 5*A*) (19, 30, 31). As described above, the known *N*-oxidases FzmM and CreE are *bona fide* members of this protein family; however, they are only distantly related to HpxL and PcxL and do not fall within the top 500 homologs shown in Fig. 5*A*. Indeed, the BLAST search results using HpxL as the query must be extended to include the top 5000 hits before FzmM and CreE are included.

Table 4
Initial rate kinetics for HpxL and PcxL
Rates were determined by monitoring NADPH consumption via UV-visible spectrophotometer. V_{max}, K_m, and K_I were determined by fitting the data with either the Michaelis-Menten (MM) or substrate inhibition (SI) model. If the data were fitted to the MM model, a K_I was not applicable (NA). Only the best fit is shown. Reaction components included: 50 mM sodium phosphate buffer, pH 7.8, 300 μM NADPH, 50 μM FAD, substrate ranging from 62.5 μM to 150 mM, and enzyme concentrations of 1 μM or 5 μM for PcxL and 5 μM or 10 μM for HpxL. The substrates used were 2AEPn (Sigma-Aldrich), synthetic (*R*)-1H2AEPn, and synthetic (*S*)-1H2AEPn. This experiment was performed in triplicate for each curve.

Enzyme	Substrate	Kinetic model	V_{max}	Apparent K_m	k_{cat}/K_m	K_I
			s^{-1}	mM	$M^{-1}\ s^{-1}$	mM
PcxL	2AEPn	MM	1.22 ± 0.02	3.3 ± 0.5	370	NA
	(*R*)-1H2AEPn	MM	0.39 ± 0.01	0.48 ± 0.02	810	NA
	(*S*)-1H2AEPn	MM	0.32 ± 0.03	6 ± 1	53	NA
HpxL	2AEPn	MM	0.032 ± 0.002	4.3 ± 0.8	7.4	NA
	(*R*)-1H2AEPn	SI	0.06 ± 0.03	4 ± 2	15	2 ± 1
	(*S*)-1H2AEPn	MM	0.039 ± 0.001	0.39 ± 0.03	100	NA

We performed a similar analysis using previously identified phosphonate biosynthetic gene clusters as the starting point (19). 23% of the phosphonate gene cluster families contain a HpxL homolog, with only three families having characterized products: phosphonocystoximic acids, hydroxyphosphonocystoximic acids, and fosfazinomycins. Thus, at least 15 novel uncharacterized phosphonic acid natural-product biosynthetic pathways encode an HpxL homolog. Based on the similarity of these enzymes within the *N*-oxidase tree, we can predict that these 15 novel phosphonic acids will likely involve the oxidation of 2AEPn or 1H2AEPn to form an oxime-containing natural product.

Discussion

PcxL and HpxL are 2AEPn and 1H2AEPn amine oxygenases

The data presented here show that PcxL and HpxL are novel FAD- and NADPH-dependent oxime-forming amine oxygenases that utilize amine-containing phosphonate substrates. Although these enzymes were shown to oxidize several small amino phosphonates, the substrate preferences of the two enzymes support the proposed biosynthetic pathways shown in Fig. 2. Accordingly, we expected that the substrate preference of the *N*-oxidases would be influenced by the presence of the proposed 2AEPn dioxygenase, HpxV, in the gene cluster of *S. regensis* NRRL WC-3744 (Fig. 2, Fig. S1, and Table S1), with HpxL having a preference for (*S*)-1H2AEPn and PcxL having a preference for 2AEPn (19). The finding that the catalytic efficiency of HpxL is 10-fold higher for (*S*)-1H2AEPn than the other substrates tested was fully consistent with this model. Our conclusions regarding PxcL are less certain, because the enzyme displays a similar catalytic efficiency with both 2AEPn

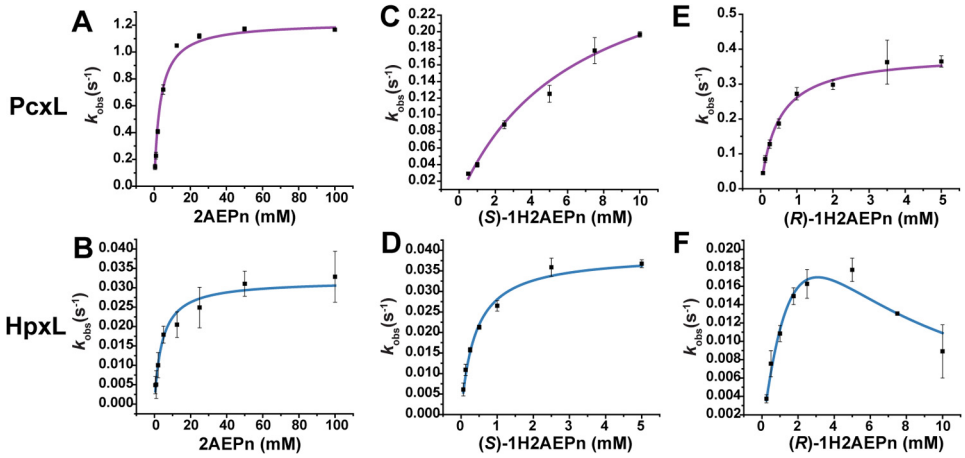

Figure 4. Kinetic curves for PcxL and HpxL in the presence of different substrates. PcxL (*A*) and HpxL (*B*) with 2AEPn as the substrate were fit to a standard Michaelis-Menten model. PcxL (*C*) and HpxL (*D*) with (*S*)-1H2AEPn were fit to a standard Michaelis-Menten model. PcxL (*E*) with (*R*)-1H2AEPn as a substrate was fit to a standard Michaelis-Menten model, and HpxL (*F*) with (*R*)-1H2AEPn as substrate was fit to the substrate inhibition model. Extracted kinetic constants are shown in Table 4.

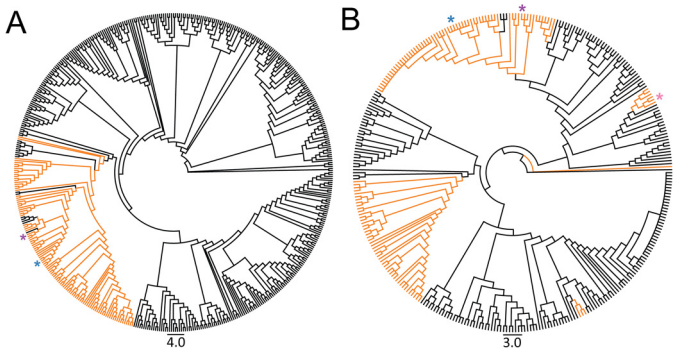

Figure 5. Cladograms showing the phylogenetic distribution of putative *N*-oxidases related to HpxL and PcxL. *A*, phylogeny of the 500 closest HpxL homologs. *hpxL*-containing gene clusters that also contain *pepM* are highlighted in *orange*. *B*, phylogeny of actinobacterial PepM sequences. *pepM*-containing gene clusters that contain an HpxL homolog are highlighted in *orange*. HpxL is denoted with a *blue asterisk*, PcxL is denoted with a *purple asterisk*, and FzmM is denoted with a *pink asterisk*. Gene clusters were arbitrarily defined to include the 15 genes upstream or downstream of the *N*-oxidase.

and (*R*)-1H2AEPn. Nevertheless, it is very likely that 2AEPn is the natural substrate given the absence of known genes to produce hydroxylated phosphonate substrates in *Streptomyces* sp. NRRL S-481.

The stoichiometry of the reaction suggests overoxidation of substrate during formation of the aldoxime

Based on the finding that NADPH and O_2 are always consumed in a 1:1 ratio by PcxL and HpxL (Table 3), oxime formation should require two separate hydroxylation steps, each consuming 1 molar equivalent of NADPH and 1 molar equivalent of oxygen. Each step would also produce 1 molar equivalent of H_2O by the reduction of O_2 with NADPH. We predict that this reaction will proceed through hydroxyamino and dihydroxyamino intermediates, with subsequent loss of water producing a nitroso intermediate, which would tautomerize to afford the final aldoxime product observed in our reactions (Fig. 6). An infrequent, third NADPH- and O_2-dependent hydroxylation of the dihydroxyamino/nitroso intermediates, or the oxime products, would then afford small amounts of the nitro derivatives seen in our data (Fig. 3 and Figs. S3–S6). The fact that we see substantially higher levels of O_2 consumption relative to aldoxime formation is consistent with this idea, as is the observation of NADPH oxidation in the absence of phosphonate substrates (*i.e.* the uncoupled reaction). We expect that the latter would produce hydrogen peroxide, although this was not tested directly.

PcxL and HpxL are new members of a class of flavin-dependent amine oxidases common in nature

Sequence analysis shows that HpxL and PcxL are members of a very large protein family that is widely distributed in bacteria. Only four members of this family have been characterized biochemically, including HpxL, PcxL, and the distantly related enzymes FzmM and CreE. Although the former, HpxL and PcxL, oxidize amino phosphonates to aldoximes (and small amounts of nitro derivatives), the latter oxidize aspartate to nitrosuccinic acid (22, 23). Given the phylogenetic distance between these distant homologs, it seemed reasonable to assume that most members of the family are amine oxidases. Interestingly, members of this presumptive amine oxidase family are common in actinobacterial phosphonate biosynthetic gene clusters, with nearly one-fourth of those examined containing a homolog. These enzymes are widely distributed on the PepM maximum-likelihood tree, suggesting that HpxL and PcxL homologs were recruited into phosphonic acid biosynthetic gene clusters multiple times; however, all of these homologs are closely related, falling into the same clade within the amine oxidase tree (Fig. 5*A*). Moreover, each of the gene clusters containing these homologs also contains the biosynthetic machinery needed to make 2AEPn or 1H2AEPn. Taken together, these data suggest that numerous phosphonate biosynthetic pathways include **1** or **3** as early intermediates (see Fig. 3). Thus, although the phosphonocystoximates are the only known oxime-containing phosphonate natural products, it seems certain that numerous additional examples await discovery.

Experimental procedures

General procedures

Nuclear magnetic resonance (NMR) spectra were collected using an Agilent Technologies 600-MHz NMR spectrometer with D_2O as the lock solvent (minimum 20% v/v). All chemicals

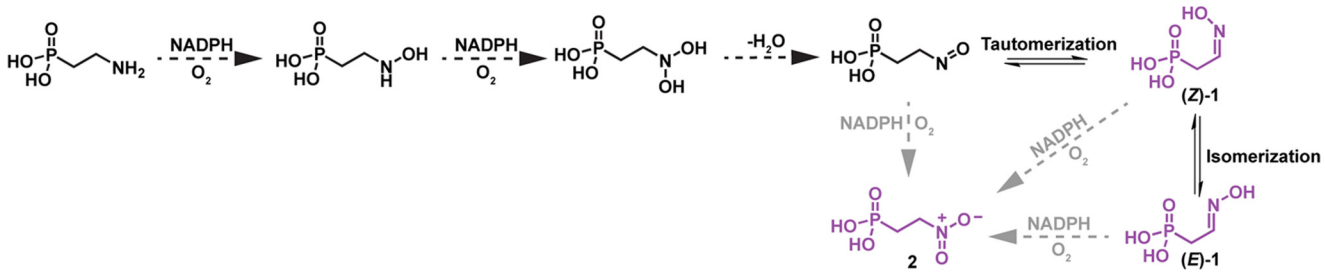

Figure 6. Proposed stepwise oxidation of 2AEPn to yield 1 or 2. This may explain the 1:2.5 substrate:NADPH ratio observed for oxime formation *in vitro*. We propose that each *N*-oxidation would require 1 molar equivalent of NADPH and molecular oxygen. This would require two *N*-oxidations and a dehydration to yield 2-nitrosoethylphosphonic acid, which could tautomerize to form 2-hydroxyiminoethylphosphonic acid. An enzyme-catalyzed overoxidation of either 2-nitrosoethylphosphonic acid or 2-hydroxyiminoethylphosphonic acid could potentially yield 2-nitroethylphosphonic acid (shown by *gray arrows*). Compounds shown in *purple* are all products observed in the reactions catalyzed by HpxL and PcxL using 2AEPn as the substrate (Fig. 3).

used in this study were purchased from Sigma-Aldrich unless otherwise noted.

N-Oxidase cloning, overexpression, and purification

The genes encoding the *N*-oxidases were amplified via PCR using primer pairs MG140 (5′-CTGGTGCCGCGCGGCAGC-CATATGacgaccgacaattccccagcca-3′) and MG141 (5′-AGT-GGTGGTGGTGGTGGTGCTCGAGtcatgcgggggtcctttcgatg-tcc-3′) for *hpxL* and primer pairs MG142 (5′-CTGGTGCCG-CGCGGCAGCCATATGcgttccaaccgactcgccatcgtcg-3′) and MG143 (5′-AGTGGTGGTGGTGGTGGTGCTCGAGtcacac-tcccgtggtgatgcgcgcg-3′) for *pcxL* from fosmids containing the phosphonocystoximic acid gene clusters (19). The plasmid pET28B was amplified using primers pET28-NdeI-R (5′-CATATGGCTGCCGCGCGGCACCAGGCCGCTG-3′) and pET28B-XhoI-F (5′-CTCGAGCACCACCACCACCACCAC-TGAGATCCGG-3′). The uppercase letters represent sequence homology to the plasmid pET28B, the underlined sequences represent inserted restriction enzyme sites, and the lowercase letters represent sequence homology to the gene to be amplified. The primer pair MG140 and MG141 was designed to mutate the GTG start codon of *hpxL* to an ATG start codon for expression in *E. coli*. The gene fragments were subsequently cloned into pET28B using Gibson Assembly® (New England Biolabs, Ipswich, MA) to yield pMNG016 for *hpxL* and pMNG017 for *pcxL*. The sequences were verified at the University of Illinois Urbana-Champaign Core Sequencing Facility.

The PcxL and HpxL proteins were affinity-purified after expression in *E. coli*. PcxL and HpxL were overexpressed in transformed *E. coli* Rosetta DE3 cells containing either plasmid pMNG016 or pMNG017. Proteins were purified using one of two methods. Method 1 involved cells grown in Studier's ZYM5052 autoinduction medium (32) with the following modification. The trace elements solution was replaced with 1 mg/liter of each iron(II) sulfate heptahydrate, zinc(II) sulfate heptahydrate, and manganese(II) chloride dihydrate. The cultures were shifted to 18 °C when absorbance (A_{600}) reached 0.6–0.8 and the protein was overexpressed for 16 h. Cells were collected via centrifugation and resuspended in lysis buffer (300 mM sodium chloride, 50 mM sodium phosphate (dibasic), 10% glycerol, and 10 mM imidazole, pH 8.0). The cell suspension was mixed with 1 mg/ml lysozyme, 100 units of DNase I, and 100 μg of RNase A for 30 min at 4 °C. The cell suspension was passed twice through a French press cell disruptor (Thermo Electron Corp., Waltham, MA) at 1000 psi. The suspension was centrifuged at 14,000 × *g* for a minimum of 30 min, and the pellet was discarded. The liquid portion was passed over a 5-ml HisTrap FPLC protein column (GE Healthcare Life Sciences) and washed with lysis buffer until the protein was no longer eluting from the column as determined by absorbance at $A_{260\ nm}$. Protein was eluted from the column on an ÄTKApurifier FPLC (GE Healthcare Life Sciences) using a gradient from 10 to 250 mM imidazole with 60 column volumes over 1 h at a flow rate of 5 ml/min. Fractions containing purified protein, as determined by running the samples on a SDS-PAGE, were pooled and concentrated using a 30-kDa molecular mass Amicon® Ultra spin filter (EMD Millipore, Burlington, MA). Method 2 involved cells grown in Luria broth until the absorbance (A_{600}) reached 0.6–0.8. The cultures were chilled on ice for 30 min, and protein expression was induced upon the addition of isopropyl β-D-1-thiogalactopyranoside to a final concentration of 1 mM. Cells were shaken at 18 °C for 16 h after induction. Pelleted cells were resuspended in lysis buffer (see above) containing 1 mg/ml lysozyme, 100 units of DNase I, and 100 μg of RNase A and mixed at 4 °C for 30 min. The cell suspension was passed twice through a French press cell disruptor (Thermo Electron Corp.) at 1000 psi. The suspension was centrifuged at 14,000 × *g* for 30 min, and the pellet was discarded. The soluble fraction containing soluble protein was mixed with 5 ml of loose nickel–nitrilotriacetic acid resin for 30 min at 4 °C. The resin was washed with wash buffer (300 mM sodium chloride, 50 mM sodium phosphate (dibasic), 10% glycerol, and 20 mM imidazole, pH 8.0) until protein was no longer eluting from the resin as determined by absorbance at $A_{260\ nm}$. Protein was eluted from the column by incubating the resin with elution buffer (300 mM sodium chloride, 250 mM sodium phosphate (dibasic), 10% glycerol, and 20 mM imidazole, pH 8.0) for 15 min and collecting the flow-through. This flow-through was concentrated using a 30-kDa molecular mass Amicon® Ultra spin filter (EMD Millipore). All samples, regardless of which purification method was used, were exchanged into storage buffer (300 mM sodium chloride, 50 mM sodium phosphate (dibasic), and 10% glycerol) using a PD-10 desalting column (GE Healthcare Life Sciences).

Bioinformatics characterization of HpxL and PcxL

The following amino acid sequences were downloaded from NCBI: HpxL (accession number WP_030990682.1), PcxL (accession number WP_051704824.1), AzmF (accession num-

ber AMQ23503.1), ClmM (accession number CCC55915.1), CrmH (accession number AFD30961.1), AlmD (accession number CCA29200.1), FzmM (accession number WP_053787792.1), and CreE (accession number ALA99202.1). These sequences were aligned using the standard settings for a MUSCLE alignment using Geneious (Geneious version 8.1.2 (33)), which provided the percent identity between the proteins shown in Table 1.

Cofactor preference of the PcxL and HpxL

Cofactor preference experiments were monitored using a Cary 4000 UV-visible spectrophotometer (Agilent Technologies, Santa Clara, CA). NADH and NADPH consumption was monitored by observing the absorption at 340 nm. Reaction components included: 50 mM sodium phosphate buffer, pH 7.8, 300 μM nicotinamide cofactor (either NADPH or NADH), 50 μM flavin cofactor (FAD or FMN), 10 mM 2AEPn, and 10 μM *N*-oxidase (PcxL or HpxL). Reaction components except for substrate and enzyme were mixed in a 200-μl quartz cuvette. Enzyme was added, and the background rate of the enzyme was collected for approximately 1 min. Reactions were initiated upon addition of 2AEPn, and three replicates were collected for each condition.

Flavin identification

LC/MS detection of flavin—HpxL (13.8 mg) and PcxL (5.4 mg) stocks were brought to room temperature and concentrated to 50 μl using a 30-kDa molecular mass Amicon® Ultra spin filter (EMD Millipore), and the flow-through was discarded. The protein was washed six times with 500 μl of ddH_2O. After washing, the PcxL was colorless, whereas HpxL retained some bound flavin as noted by the yellow color of the protein (Fig. S2). The collected flavin was flash-frozen and placed on a lyophilizer until dry. The flavin was resuspended in ddH_2O. We determined the concentration of the flavins based on absorbance at 450 nm using the extinction coefficient of ϵ = 12,000 $M^{-1}cm^{-1}$ for FAD (HpxL-extracted flavin = 37.1 μM and PcxL-extracted flavin = 30.9 μM). The extracted flavin (10 μl) was injected onto a 150 × 4.6 mm Synergi 4-μm Fusion-RP column connected to an Agilent 1200 series LC/MSD SL mass spectrometer (Agilent) monitoring for the masses corresponding to FAD (m/z = 786.2) and FMN (m/z = 457.1) in positive mode. The following solvents were used: A = 95% ddH_2O, 5% acetonitrile with 0.1% formic acid and B = 5% ddH_2O, 95% acetonitrile with 0.1% formic acid. The sample was run with a linear gradient from times 0–12 min: time 0 min = 5% B, 12 min = 95% B, 15 min = 95% B, 18 min = 5% B, and 25 min = 5% B. The flow rate was 1 ml/min.

Absorption spectra of HpxL and PcxL—HpxL (3.6 mg) and PcxL (6.1 mg) stocks were used to determine the absorption spectra of the proteins on a Cary 4000 UV-visible spectrophotometer (Agilent) scanning from 200 to 800 nm. NADPH was added to the protein to a final concentration of 500 μM, and the absorption spectrum of the protein was measured after 1 min of incubation. Flavin that was washed away from the proteins was also measured.

Stoichiometry determination

Oxygen–NADPH ratio—Oxygen consumption was monitored on a Clark-type oxygen electrode (Hansatech Instruments, Norfolk, England). NADPH consumption was monitored (A_{340}) on a Cary 4000 UV-visible spectrophotometer (Agilent). Reaction components included 50 mM sodium phosphate buffer (air-saturated), pH 7.8, 300 μM NADPH, 50 μM FAD, 50 mM 2AEPn, and 1 μM PcxL or 5 μM HpxL. Reactions were initiated by the addition of enzyme and monitored for 5 min. Three replicates were performed on each instrument. The number of moles of both oxygen and NADPH consumed by the enzyme in 5 min was determined and compared.

NADPH–substrate ratio—NADPH consumption was determined using a Cary 4000 UV-visible spectrophotometer (Agilent) and via ^{31}P NMR. 2AEPn consumption was determined using ^{31}P NMR. The reaction components included 50 mM sodium phosphate buffer (air-saturated), pH 7.8, 3 mM NADPH, 500 μM FAD, 5 mM 2AEPn, and 25 μM PcxL or 25 μM HpxL. Three replicates were performed. The reactions were incubated for 30 min at room temperature and were quenched using 1 reaction volume of 100% methanol. Dimethylphosphinic acid was added to the reaction as an internal quantification standard to yield a final concentration of 10 mM. The number of moles of substrate and NADPH consumed was determined and directly compared.

Generation of (S)-1H2AEPn by HpxV

To yield an N-terminal His_6-tagged HpxV, hpxV was amplified using the primers Orf10_LIC_F (5′-TACTTCCAATCCAATGCAcctactcacccacgcactc-3′) and Orf10_LIC_R (5′-TTATCCACTTCCAATGTTATTActacttgctcgaccacatg-3′) and cloned into the ligation-independent cloning vector pET His_6 TEV LIC cloning vector (2B-T). The N-terminal His_6-tagged HpxV was overexpressed in transformed *E. coli* BL21 DE3 containing the pET His_6 TEV LIC cloning vector (2B-T) with *hpxV*. HpxV was overexpressed and purified using method 2 as described above. (*S*)-1H2AEPn was generated using HpxV, a 2AEPn-dependent α-ketoglutarate–dependent dioxygenase from *S. regensis* NRRL WC-3744. The reactions contained 50 mM PBS, pH 7.4, 40 mM α-ketoglutarate, 1 mM iron(II) ammonium sulfate, 7.5 mM 2AEPn, 4 mM L-ascorbic acid, and 200 μM HpxV. Reactions were incubated for 13 h at 30 °C. The reaction was quenched by precipitating the protein by the addition of methanol to yield a 90% methanol precipitation. The precipitated protein was removed via centrifugation, and the reaction mixture was concentrated on a rotary evaporator. The concentration of 1H2AEPn generated was determined by ^{31}P NMR spectroscopy using phosphite as an internal reference standard for quantification at a final concentration of 10 mM. In some experiments synthetic (*S*)-1H2AEPn was used (see below).

Product formation experiments

HpxL or PcxL were incubated with 2AEPn or HpxV-generated (*S*)-1H2AEPn to monitor which products were formed by the *N*-oxidases. The reactions were set up with the following components: 25 mM sodium phosphate buffer, pH 7.8, 500 μM NADPH, 100 μM FAD, 25 μM PcxL or HpxL, 10 μM phosphite dehydrogenase, 25 mM phosphite, and 3 mM of substrate, pH

7.8. Reactions were incubated for 16 h at room temperature. Product formation was monitored using ^{31}P NMR spectroscopy, ^{1}H NMR spectroscopy, and ^{31}P-^{1}H HMBC spectroscopy. A mutated phosphite dehydrogenase (PTDH17x) that can use either NADH or NADPH as the nicotinamide coenzyme (34) was used to regenerate NADPH in the substrate specificity experiments. This enzyme was overexpressed in *E. coli* BL21 DE3 cells containing a plasmid with PTDH17x cloned into pET15b. Cells were grown in modified Studier's ZYM5052 medium (as described above) at 37 °C until A_{600} reached 0.6–0.8, the culture was shifted to 18 °C, and the protein was overexpressed for 16 h. The cell suspension was passed twice through a French press cell disruptor (Thermo Electron Corp.) at 1000 psi. The suspension was centrifuged at 14,000 × *g* for a minimum of 30 min, and the pellet was discarded. Soluble cell lysate was passed over free nickel–nitrilotriacetic acid immobilized metal affinity chromatography (IMAC) resin and washed with wash buffer (20 mM Tris-HCl, 500 mM NaCl, and 10% glycerol (% v/v), pH 7.6). The bound protein was washed stepwise with the wash buffer containing increasing levels of imidazole at concentrations of 10, 25, and 50 mM, respectively, until there was no protein detected by monitoring $A_{260\ nm}$. Protein was eluted from the column using wash buffer containing 250 mM imidazole and concentrated using a 10-kDa molecular mass Amicon® Ultra spin filter (EMD Millipore). The protein was exchanged into protein storage buffer (50 mM HEPES, 200 mM KCl, and 10% glycerol (% v/v), pH 7.5) using a PD-10 desalting column (GE Healthcare Life Sciences).

Stereospecific synthesis of (R)- and (S)-1H2AEPn

Enantiopure (enantiomeric excess (ee) > 99%) (*R*)- and (*S*)-1H2AEPn was generated following previously published methods (35).

Kinetic assays

Enzyme assays were monitored using a Cary 4000 UV-visible spectrophotometer (Agilent). NADPH consumption was monitored by observation of the absorption at 340 nm. Reaction components included: 50 mM sodium phosphate buffer, pH 7.8, 300 μM NADPH, 50 μM FAD, substrate concentrations ranging from 62.5 μM to 150 mM, and enzyme concentrations of 1 or 5 μM for PcxL and 5 or 10 μM for HpxL. Briefly, the reaction components except for substrate and enzyme were mixed in a 200-μl quartz cuvette. Enzyme was added, and the background rate of the enzyme was collected for approximately 1 min. Reactions were initiated upon the addition of substrate. Three replicates were obtained for each concentration of substrate. Because of the time it takes to complete 1 NADPH consumption curve for HpxL (between 15 and 30 min), all of the initial rates are approximate initial rates. The rate over ~30 s once the enzyme reaches steady state was read, and this was used as the "initial rate."

Construction of phylogenetic trees and assignment of genomic neighborhoods

To construct the *N*-oxidase phylogenetic tree, the top 500 BLAST (36) hits obtained using HpxL (WP_030990672.1) as a query sequence were downloaded on February 18th, 2017. These sequences were aligned using MAFFT with default settings (37), and the maximum likelihood tree was constructed with FastTree using default settings (38). The accession numbers of the 500 amino acid sequences used in the tree were run through RODEO (29) to identify the putative *N*-oxidase proteins involved in a phosphonate gene cluster. A positive hit constitutes a phosphoenolpyruvate mutase enzyme being within 15 genes upstream or downstream of the *N*-oxidase.

To construct the PepM phylogenetic tree, five Actinobacteria PepM amino acid sequences were used as a BLAST query (19): *Streptomyces luridus* PepM (ACZ13456), *Streptomyces viridochromogenes* (AAU00071), *Streptomyces fradiae* (ACG70831), *Strepomyces rubellomurinus* (ABB90393), and *S. regensis* HpxU (WP_030646403.1). The search was limited to Actinobacteria, with Mycobacteria excluded from the search due the presence of large numbers of isocitrate lyase family proteins that lack the diagnostic PepM motif. All hits for each search were sorted to remove duplicates, and the characteristic EDK*xxxxx*NS motif was identified manually to distinguish actual PepM sequences from other members of the isocitrate lyase superfamily (39). There were 199 amino acid sequences identified as putative PepM sequences using this approach. These amino acid sequences were aligned using MAFFT (37), and the maximum likelihood tree was constructed using FastTree (38). RODEO (29) was used to identify phosphonate gene clusters that contain an *N*-oxidase homolog. A positive hit constitutes an *N*-oxidase being within 15 genes upstream or downstream of the PepM.

Author contributions—M. N. G., J. P. C., K. S. J., K. P., and W. W. M. conceptualization; M. N. G., J. P. C., and W. W. M. data curation; M. N. G., J. P. C., and W. W. M. formal analysis; M. N. G. and W. W. M. supervision; K. P. and W. W. M. funding acquisition; M. N. G., J. P. C., K. S. J., K. P., and W. W. M. investigation; M. N. G. and W. W. M. visualization; M. N. G., J. P. C., K. S. J., K. P., and W. W. M. methodology; M. N. G., J. P. C., and W. W. M. writing-original draft; M. N. G. and W. W. M. project administration; M. N. G., J. P. C., and W. W. M. writing-review and editing; K. P. and W. W. M. resources.

Acknowledgments—We thank N. Petronikolou for constructing the HpxV expression vector. NMR spectroscopy data collected in this study was done at the Carl R. Woese Institute for Genomic Biology Core Facilities on a 600-MHz NMR funded by National Institutes of Health Grant S10-RR028833.

References

1. Kelly, W. L., and Townsend, C. A. (2002) Role of the cytochrome P450 NocL in nocardicin A biosynthesis. *J. Am. Chem. Soc.* **124,** 8186–8187 CrossRef Medline
2. Jang, J. H., van Soest, R. W., Fusetani, N., and Matsunaga, S. (2007) Pseudoceratins A and B, antifungal bicyclic bromotyrosine-derived metabolites from the marine sponge *Pseudoceratina purpurea*. *J. Org. Chem.* **72,** 1211–1217 CrossRef Medline
3. Bacher, M., Brader, G., Hofer, O., and Greger, H. (1999) Oximes from seeds of *Atalantia ceylanica*. *Phytochemistry* **50,** 991–994 CrossRef
4. Moya, P., Castillo, M., Primo-Yúfera, E., Couillaud, F., Martínez-Máñez, R., Garcerá, M. D., Miranda, M. A., Primo, J., and Martínez-Pardo, R. (1997) Brevioxime: A new juvenile hormone biosynthesis inhibitor iso-

lated from *Penicillium brevicompactum*. *J. Org. Chem.* **62,** 8544–8545 CrossRef Medline
5. Hong, S., Shin, Y., Jung, M., Ha, M. W., Park, Y., Lee, Y. J., Shin, J., Oh, K. B., Lee, S. K., and Park, H. G. (2015) Efficient synthesis and biological activity of psammaplin A and its analogues as antitumor agents. *Eur. J. Med. Chem.* **96,** 218–230 CrossRef Medline
6. Kim, Y. S., Jeong, H. Y., Kim, A. R., Kim, W. H., Cho, H., Um, J., Seo, Y., Kang, W. S., Jin, S. W., Kim, M. C., Kim, Y. C., Jung, D. W., Williams, D. R., and Ahn, Y. (2016) Natural product derivative BIO promotes recovery after myocardial infarction via unique modulation of the cardiac microenvironment. *Sci. Rep.* **6,** 30726 CrossRef Medline
7. Eyer, P. (2003) The role of oximes in the management of organophosphorus pesticide poisoning. *Toxicol. Rev.* **22,** 165–190 CrossRef Medline
8. Wong, L., Radic, Z., Brüggemann, R. J., Hosea, N., Berman, H. A., and Taylor, P. (2000) Mechanism of oxime reactivation of acetylcholinesterase analyzed by chirality and mutagenesis. *Biochemistry* **39,** 5750–5757 CrossRef Medline
9. Halkier, B. A., and Gershenzon, J. (2006) Biology and biochemistry of glucosinolates. *Annu. Rev. Plant Biol.* **57,** 303–333 CrossRef Medline
10. Chen, H. P., Zhao, Z. Z., Li, Z. H., Dong, Z. J., Wei, K., Bai, X., Zhang, L., Wen, C. N., Feng, T., and Liu, J. K. (2016) Novel natural oximes and oxime esters with a vibralactone backbone from the basidiomycete *Boreostereum vibrans*. *ChemistryOpen* **5,** 142–149 CrossRef Medline
11. Arabshahi, L., and Schmitz, F. J. (1987) Brominated tyrosine metabolites from an unidentified sponge. *J. Org. Chem.* **52,** 3584–3586 CrossRef
12. Du, L., Lykkesfeldt, J., Olsen, C. E., and Halkier, B. A. (1995) Involvement of cytochrome P450 in oxime production in glucosinolate biosynthesis as demonstrated by an *in vitro* microsomal enzyme system isolated from jasmonic acid-induced seedlings of *Sinapis alba* L. *Proc. Natl. Acad. Sci. U.S.A.* **92,** 12505–12509 CrossRef Medline
13. Bennett, R., Donald, A., Dawson, G., Hick, A., and Wallsgrove, R. (1993) Aldoxime-forming microsomal enzyme systems involved in the biosynthesis of glucosinolates in oilseed rape (*Brassica napus*) leaves. *Plant Physiol.* **102,** 1307–1312 CrossRef Medline
14. Bennett, R. N., Kiddle, G., Hick, A. J., Dawson, G. W., and Wallsgrove, R. M. (1996) Distribution and activity of microsomal NADPH-dependent monooxygenases and amino acid decarboxylases in cruciferous and non-cruciferous plants, and their relationship to foliar glucosinolate content. *Plant Cell Environ.* **19,** 801–812 CrossRef
15. Kelly, W. L., and Townsend, C. A. (2005) Mutational Analysis of nocK and nocL in the nocardicin A producer *Nocardia uniformis*. *J. Bacteriol.* **187,** 739–746 CrossRef Medline
16. Cortina, N. S., Revermann, O., Krug, D., and Müller, R. (2011) Identification and characterization of the althiomycin biosynthetic gene cluster in *Myxococcus xanthus* DK897. *ChemBioChem* **12,** 1411–1416 CrossRef Medline
17. Liu, N., Song, L., Liu, M., Shang, F., Anderson, Z., Fox, D. J., Challis, G. L., and Huang, Y. (2016) Unique post-translational oxime formation in the biosynthesis of the azolemycin complex of novel ribosomal peptides from *Streptomyces* sp. FXJ1.264. *Chem. Sci.* **7,** 482–488 Medline
18. Zhu, Y., Zhang, Q., Li, S., Lin, Q., Fu, P., Zhang, G., Zhang, H., Shi, R., Zhu, W., and Zhang, C. (2013) Insights into caerulomycin A biosynthesis: A two-component monooxygenase CrmH-catalyzed oxime formation. *J. Am. Chem. Soc.* **135,** 18750–18753 CrossRef Medline
19. Ju, K. S., Gao, J., Doroghazi, J. R., Wang, K. K., Thibodeaux, C. J., Li, S., Metzger, E., Fudala, J., Su, J., Zhang, J. K., Lee, J., Cioni, J. P., Evans, B. S., Hirota, R., Labeda, D. P., van der Donk, W. A., van der, Metcalf, W. W. (2015) Discovery of phosphonic acid natural products by mining the genomes of 10,000 actinomycetes. *Proc. Natl. Acad. Sci. U.S.A.* **112,** 12175–12180 CrossRef Medline
20. Cioni, J. P., Doroghazi, J. R., Ju, K. S., Yu, X., Evans, B. S., Lee, J., and Metcalf, W. W. (2014) Cyanohydrin phosphonate natural product from *Streptomyces regensis*. *J. Nat. Prod.* **77,** 243–249 CrossRef Medline
21. Kelley, L. A., Mezulis, S., Yates, C. M., Wass, M. N., and Sternberg, M. J. (2015) The Phyre2 web portal for protein modeling, prediction and analysis. *Nat. Protoc.* **10,** 845–858 CrossRef Medline
22. Sugai, Y., Katsuyama, Y., and Ohnishi, Y. (2016) A nitrous acid biosynthetic pathway for diazo group formation in bacteria. *Nat. Chem. Biol.* **12,** 73–75 CrossRef Medline
23. Huang, Z., Wang, K. A., and van der Donk, W. A. (2016) New insights into the biosynthesis of fosfazinomycin. *Chem. Sci.* **7,** 5219–5223 CrossRef Medline
24. Lin, J., and Cashman, J. R. N-Oxygenation of Phenethylamine to the trans-oxime by adult human liver flavin-containing monooxygenase and retroreduction of phenethylamine hydroxylamine by human liver microsomes. *J. Pharmacol. Exp. Ther.* **282,** 1269–1279
25. Walsh, C. T., and Wencewicz, T. A. (2013) Flavoenzymes: Versatile catalysts in biosynthetic pathways. *Nat. Prod. Rep.* **30,** 175–200 Medline
26. Pretsch, E., Buhlmann, P., and Badertscher, M. (2009) *Structure Determination of Organic Compounds*, 4th Ed., p. 209, Springer-Verlag, Berlin
27. Pallitsch, K., Happl, B., and Stieger, C. (2017) Determination of the absolute configuration of (-)-hydroxynitrilaphos and related biosynthetic questions. *Chem. Eur. J.* **23,** 15655–15665 CrossRef Medline
28. Anderson, V. E., Weiss, P. M., and Cleland, W. W. (1984) Reaction intermediate analogs for enolase. *Biochemistry.* **23,** 2779–2786 CrossRef Medline
29. Tietz, J. I., Schwalen, C. J., Patel, P. S., Maxson, T., Blair, P. M., Tai, H. C., Zakai, U. I., and Mitchell, D. A. (2017) A new genome-mining tool redefines the lasso peptide biosynthetic landscape. *Nat. Chem. Biol.* **13,** 470–478 CrossRef Medline
30. Metcalf, W. W., and van der Donk, W. A. (2009) Biosynthesis of phosphonic and phosphinic acid natural products. *Annu. Rev. Biochem.* **78,** 65–94 CrossRef Medline
31. Yu, X., Doroghazi, J. R., Janga, S. C., Zhang, J. K., Circello, B., Griffin, B. M., Labeda, D. P., and Metcalf, W. W. (2013) Diversity and abundance of phosphonate biosynthetic genes in nature. *Proc. Natl. Acad. Sci. U.S.A.* **110,** 20759–20764 CrossRef Medline
32. Studier, F. W. (2005) Protein production by auto-induction in high density shaking cultures. *Protein Expr. Purif.* **41,** 207–234 CrossRef Medline
33. Kearse, M., Moir, R., Wilson, A., Stones-Havas, S., Cheung, M., Sturrock, S., Buxton, S., Cooper, A., Markowitz, S., Duran, C., Thierer, T., Ashton, B., Meintjes, P., and Drummond, A. (2012) Geneious Basic: An integrated and extendable desktop software platform for the organization and analysis of sequence data. *Bioinformatics* **28,** 1647–1649 CrossRef Medline
34. Woodyer, R. D., Shao, Z., Thomas, P. M., Kelleher, N. L., Blodgett, J. A., Metcalf, W. W., van der Donk, W. A., and Zhao, H. (2006) Heterologous production of fosfomycin and identification of the minimal biosynthetic gene cluster. *Chem. Biol.* **13,** 1171–1182 CrossRef Medline
35. van Staalduinen, L. M., McSorley, F. R., Schiessl, K., Séguin, J., Wyatt, P. B., Hammerschmidt, F., Zechel, D. L., and Jia, Z. (2014) Crystal structure of PhnZ in complex with substrate reveals a di-iron oxygenase mechanism for catabolism of organophosphonates. *Proc. Natl. Acad. Sci. U.S.A.* **111,** 5171–5176 CrossRef Medline
36. Altschul, S. F., Gish, W., Miller, W., Myers, E. W., and Lipman, D. J. (1990) Basic local alignment search tool. *J. Mol. Biol.* **215,** 403–410 CrossRef Medline
37. Katoh, K., and Standley, D. M. (2013) MAFFT multiple sequence alignment software version 7: Improvements in performance and usability. *Mol. Biol. Evol.* **30,** 772–780 CrossRef Medline
38. Price, M. N., Dehal, P. S., and Arkin, A. P. (2010) FastTree 2: Approximately maximum-likelihood trees for large alignments. *PLoS ONE* **5,** e9490 CrossRef Medline
39. Chen, C. M., Ye, Q. Z., Zhu, Z. M., Wanner, B. L., and Walsh, C. T. (1990) Molecular biology of carbon-phosphorus bond cleavage. Cloning and sequencing of the *phn* (psiD) genes involved in alkylphosphonate uptake and C-P lyase activity in *Escherichia coli* B. *J. Biol. Chem.* **265,** 4461–4471 Medline
40. Garcia, I., Vior, N. M., González-Sabín, J., Braña, A. F., Rohr, J., Moris, F., Méndez, C., and Salas, J. A. (2013) Engineering the biosynthesis of the polyketide-nonribosomal peptide collismycin A for generation of analogs with neuroprotective activity. *Chem. Biol.* **20,** 1022–1032 CrossRef Medline